INSERTION DEVICES CHARACTERIZATION AT THE SLS 2.0

S. Bettoni*,[1], M. Aiba[1], F. Armborst[1], M. Calvi[2], J. Kallestrup[1], D. Zimoch[1]
[1]PSI Center for Accelerator Science and Engineering, Villigen, Switzerland
[2]PSI Center for Photon Science, Villigen, Switzerland

Abstract

Accurate measurement of high-order multipoles in insertion devices is crucial for meeting the beam-dynamics requirements of Swiss Light Source 2.0 (SLS 2.0). A beam-based method using transverse tune-shift measurements can effectively identify sextupole, octupole, and higher-order magnetic components under normal operating conditions, avoiding the need for dedicated magnetic tests. Among the upgraded insertion devices – planar, in-vacuum, and knot-type – only the knot-type device shows significant multipole components beyond sextupole, reaching octupole order. This study focuses on the knot-type device, which is expected to be used in SLS 2.0 and in other modern synchrotron facilities, presenting measurements and comparisons with simulation results.

THE INSERTION DEVICES AT SLS 2.0

The Swiss Light Source 2.0 (SLS 2.0) is a 2.7 GeV fourth generation synchrotron light source currently being commissioned at the Paul Scherrer Institute [1]. The machine lattice is based on a seven-bend achromat scheme including both longitudinal and reverse bends to achieve a very low emittance. The storage ring hosts various insertion devices (IDs), some reused and others newly developed, including in-vacuum planar IDs and advanced APPLE-X knot IDs. Hard X-ray performance is improved with shorter period, more powerful in-house-built in-vacuum undulators. Soft X-ray beamlines now use APPLE-X-knot undulators [2] – based on the design from the SwissFEL Athos beamline [3] – which allow full polarization control and reduce the central heat load. Their advanced "knot" magnetic structure [4–6] also suppresses unwanted higher-order harmonics, improving optical performance and energy resolution. The IDs may introduce higher-order multipole field components affecting the optics, dynamic aperture [7], and beam lifetime. A careful evaluation and correction of these effects is essential to optimize the performance of the machine. In SLS 2.0, the highest multipole order magnet installed and which can be used to control the non-linear optics of the machine is the octupole. Consequently, compensating multipole components beyond the octupole order in the undulators is not straightforward. This is the first time that this kind of ID is installed in a synchrotron, where high resolution beam-based measurements are possible, using the fact that the beam passes through the ID many thousands of times, allowing for a more precise determination of the higher-order multipoles compared to what is possible in a single-pass machine. Beam-based measurements in 2025 showed all IDs have multipoles no higher than sextupole, except the UE36 knot-type (Apple-X) device, which exhibits more significant higher-order complexity.

* simona.bettoni@psi.ch

MODELING

We generated a high-resolution 3D magnetic field map using RADIA [8] with longitudinal step size of 0.5 mm along the longitudinal z-axis, and transverse steps of 20 µm spanning from -2 mm to +2 mm and from -0.2 mm to +0.2 mm in the horizontal (x) and vertical (y) direction, respectively. The asymmetry of the grid range in the transverse plane is due to the fact that we restrict ourselves to the analysis of the normal multipoles in this proceeding. Since the multipoles have to be computed around the reference trajectory at the location $(z, x_{\mathrm{TR}}, y_{\mathrm{TR}})$, the first step of the analysis is the determination of such a trajectory. The transverse particle motion is obtained through a stepwise integration of the field along z. At each step, the transverse angles x' and y' are updated using the local magnetic field components according to:

$$x'_i = x'_{i-1} + \frac{1}{B_\rho} B_y \, \Delta z, \qquad y'_i = y'_{i-1} + \frac{1}{B_\rho} B_x \, \Delta z, \quad (1)$$

where B_ρ is the magnetic rigidity, and B_x, B_y are the transverse magnetic field components evaluated at the particle location at the preceding step. The transverse positions are subsequently updated using the angles:

$$x_i = x_{i-1} + x'_i \, \Delta z, \qquad y_i = y_{i-1} + y'_i \, \Delta z \quad (2)$$

assuming that the angle is sufficiently small to approximate its tangent with itself. Since the field map does not include corrections of the first and second field integrals, appropriate initial conditions in both position and angle must be determined. These are obtained by minimizing the trajectory deviations. Figure 1 shows a comparison between the uncorrected trajectory in the mid-plane and the optimized trajectory obtained by adjusting the initial conditions at the entrance of the ID. In the machine, this procedure corresponds to locally tuning the beam orbit in the ID region using dedicated orbit correctors. The situation is significantly less critical in the vertical plane, where the maximum beam excursion remains below 5 µm.

Following the procedure described in [9] and [10], we expand the vertical component of the magnetic field at longitudinal position z in a reference frame co-propagating with the beam as:

$$\begin{aligned} B_y(x,s) &= \sum_{n=0}^{\infty} \frac{1}{n!} \left. \frac{\partial^n B_y(x,s)}{\partial x^n} \right|_{x=x_{\mathrm{tr}}} (x - x_{\mathrm{tr}})^n \\ &\equiv \sum_{n=0}^{\infty} b_n^T (x - x_{\mathrm{tr}})^n \end{aligned} \quad (3)$$

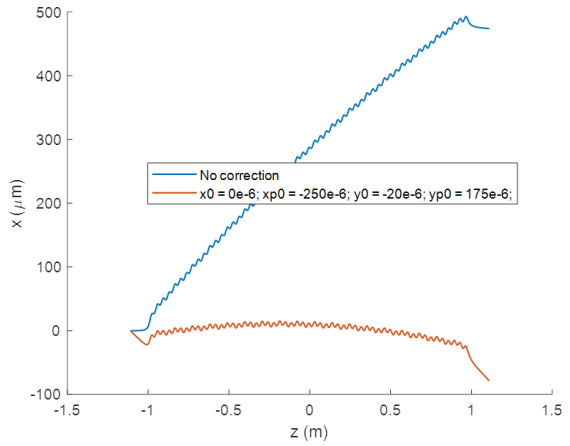

Figure 1: Orbits in the mid-plane of the ID obtained from the simulated field map, comparing the uncorrected case and the trajectory with optimized initial conditions at the entrance of the ID.

where b_n^T are the coefficients describing the different orders of the magnetic field components. For simplicity, the explicit dependence on z is omitted in the notation. These coefficients can be determined from the field map extracted from the model.

Odd terms of b_n^T degrade near the device end due to numerical artifacts. To suppress this noise, we subtract the odd multipoles computed around the magnetic axis, b_n^A, which should vanish by left–right symmetry. This improves analysis quality without increasing computational cost, as shown in Fig. 2. The integrals of b_n^T, computed as described above, are reported in the title of the corresponding subplot. As expected [9], the even terms are compensated along the ID, resulting in integrals that are two to four orders of magnitude smaller than their peak values. In contrast, for the odd terms the integrated values are comparable to their respective

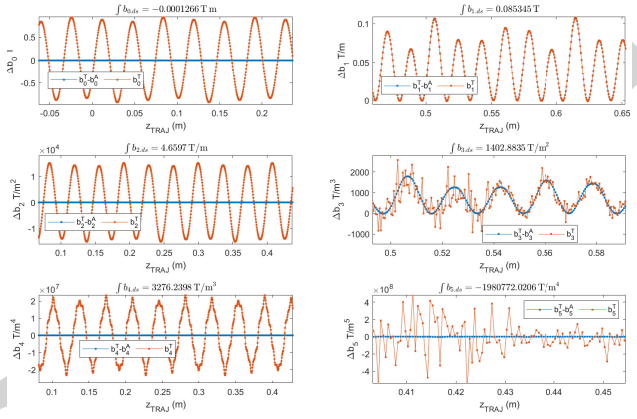

Figure 2: Evolution of the coefficients of the normal multipoles along the ID using the computed field map where the odd terms computed on-axis are used to remove the noise background from those computed with respect to the trajectory like defined in the text.

maxima. We used these coefficients to compute the corresponding high-order magnet strength expressed according to the MAD-X definition [11]:

$$K_n = \frac{1}{B\rho}\frac{\partial^n B_y}{\partial x^n}\,. \tag{4}$$

From Eqs. (3) and (4) we obtain:

$$K_n = \frac{n!}{B\rho} b_n^T\,. \tag{5}$$

Table 1 shows I_n, integrals of the polynomial coefficients b_n^T and the corresponding KL_n, integrals of K_n determined using the field map. We omit in table 1 the terms significantly

Table 1: Integrals of the multipole coefficients and corresponding KL_n values.

Multipole	Order (n)	KL_n (m^{-n})
0	Dipole	1.4×10^{-5}
1	Quadrupole	7.7×10^{-3}
2	Sextupole	1.03
3	Octupole	850.55

smaller than the maxima of b_n^T.

The tune shift as a function of the closed orbit bump amplitude by x_A can be expressed in terms of the KL_n coefficients as:

$$\Delta Q_x = f_1(\beta_x, K_1) + f_2(\beta_x, K_2)\, x_A + f_3(\beta_x, K_3)\, x_A^2, \tag{6}$$

where β_x is the average Twiss beta function along the insertion device (ID). Each multipole contributes a different polynomial order to the tune shift: constant for the quadrupole, linear for the sextupole, and quadratic for the octupole. This allows extraction of KL_n from tune shift measurements for comparison with RADIA-based model predictions.

MEASUREMENTS

Tune shifts from closed-orbit bumps provide a precise probe of lattice nonlinearities, averaging the beam's response over many turns effectively averaging out small fluctuations and enhancing the response to non-linear fields. This enables the detection of effects that would be difficult to observe in a single-pass machine. Additionally, closed orbit bumps systematically probe localized regions of the accelerator, allowing for the analysis of individual devices.

We employed the Numerical Analysis of Fundamental Frequencies (NAFF) algorithm [12, 13] in conjunction with the mixed-BPM method [14] using data from all 115 Beam Positions Monitors (BPMs) to determine the tunes. We could rely on excellent BPMs [15], and beam stability mainly due to the feedbacks and the fact that the majority of the magnets installed in the ring are permanent magnets.

In the first measurement campaign we imposed closed orbit bumps of different amplitudes around the ID, while measuring the tune and the lifetime both at the minimum and maximum ID gap. We subtracted the latter from the

former to exclude the extra tune shifts due to the sextupoles and octupoles present in the orbit bump in the analysis of the integrated multipoles.

The first approach we used for the measurements was to generate closed orbit bumps of different amplitudes around the ID while keeping both the Fast Orbit Feedback (FOFB) and the Feed-Forward (FF) table correction active. This ensured that the beam remained on the golden orbit outside the ID, thereby minimizing contributions from non-linearities in other sections of the machine.

The results of one of these measurements are shown in Fig. 3.

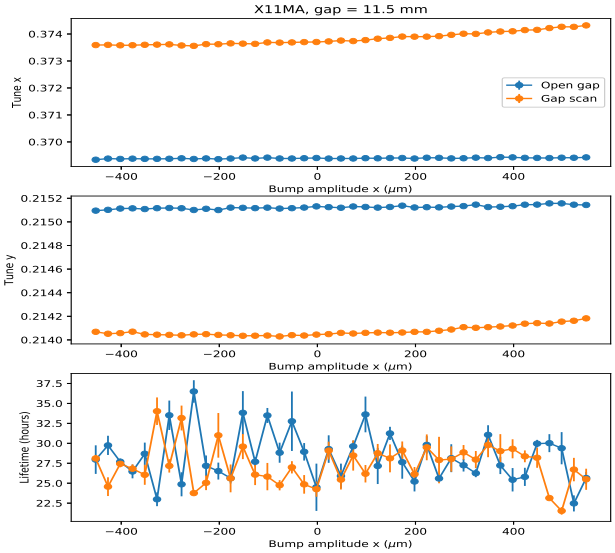

Figure 3: Tune shifts as a function of the closed orbit bump amplitude around the ID. Top: horizontal tune. Middle: vertical tune. Bottom: beam lifetime. Measurements are shown for both maximum (open) and minimum (closed) ID gaps.

In the second campaign of measurements we shifted the ID instead of performing closed orbit bumps. Figure 4 shows the difference between the tunes measured at closed and open gap as a function of horizontal shift of the ID position. We consider this as the most precise measurement we did until now, also because this was performed few days after the verification of the optics the KL_n depends on.

COMPARISON

We computed the KL_n coefficients from the field map and from tune shift measurements, as previously described. Table 2 compares these values with the minimum and maximum strengths of the corresponding magnet orders present in SLS 2.0. During the tune measurements, the tune exhibits an intrinsic linear drift, which may affect both the offset and the slope of the measured tune shift. As a result, the determination of the quadrupole component (determined from the offset of the tune shift) and the sextupole component (calculated from its slope) cannot be considered precise until this effect is corrected. However, these components

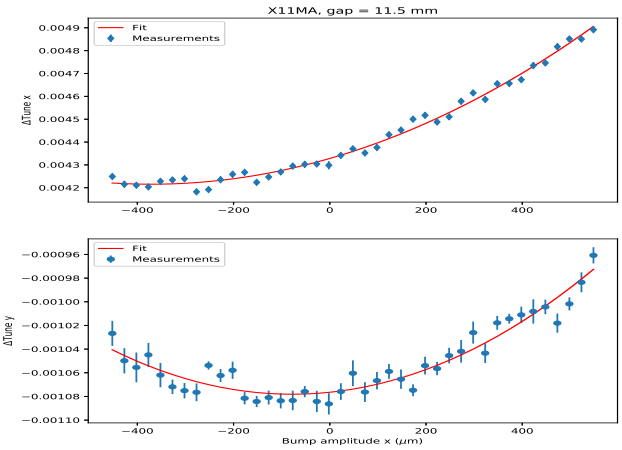

Figure 4: Tune shift as a function of the offset in the x direction of the UE36 ID with respect to the position used during the photon delivery.

Table 2: Comparison of multipole strengths in the SLS 2.0 lattice. The model values are computed from the analysis of the field map, whereas the measurement values are deduced from tune shift measurements.

Multipole	**Model (Field Map)**	**Measurement (Tune Shift)**	**Lattice**
Dipole (adim.)	1.4×10^{-5}		
Quadrupole (m^{-1})	7.7×10^{-3}	1.67×10^{-2}	0.22–1.16
Sextupole (m^{-2})	1.03	1.46	67–109
Octupole (m^{-3})	850.55	898.08	86–1900

were found to be small as predicted in the model, and their impact on the lattice is limited. The octupole component (computed from the quadratic term) agrees with the model predictions at the level of a few percent, and it is not harmful to the dynamic aperture [7]. Furthermore, no higher-order components above octupole are observed in the ID from this measurement, hence we may not need complicated compensation relying on the higher order effects from sextupoles and octupoles.

CONCLUSIONS

We have presented a beam-based characterization of the high-order multipole content of the insertion devices installed in SLS 2.0. This method provides a precise and effective approach to probe non-linear magnetic components. All investigated IDs exhibit no significant multipole components beyond the sextupole order, with the exception of the UE36 knot-type device. For this device, a measurable octupole component is observed. The comparison with the model based on RADIA field maps shows agreement at the level of a few percent for this term. The absence of higher-order multipoles beyond the octupole confirms the expectations from dynamic aperture studies and indicates that the impact of the IDs on machine performance can be effectively corrected using the available lattice elements.

REFERENCES

[1] H. Braun *et al.*, "SLS 2.0 storage ring. Technical design report", Paul Scherrer Institute, Villigen, Switzerland, Rep. No. 21-02, https://www.dora.lib4ri.ch/psi/islandora/object/psi:39635.

[2] X. Liang *et al.*, "Analysis of the first magnetic results of the PSI APPLE X undulators in elliptical polarisation", *Nucl. Instrum. Methods Phys. Res. A*, vol. 987, p. 164741, Jan. 2021. doi:10.1016/j.nima.2020.164741

[3] R. Abela *et al.*, "The SwissFEL soft X-ray free-electron laser beamline: Athos", *J. Synchrotron Radiat.*, vol. 26, part 4, pp. 1073–1084, Jul 2019. doi:10.1107/S1600577519003928

[4] F. Ji *et al.*, "Design and performance of the APPLE-Knot undulator", *J. Synchrotron Radiat.*, vol. 22, pp. 901—907, 2015. doi:10.1107/S1600577515006062

[5] F. Zhang, Z. Sun, Y. Qiao, and S. Qiao, "Practical design and performance of a new merged APPLE-Knot undulator", *J. Synchrotron Radiat.*, vol. 27, no. 6, pp. 1494—1498, 2020. doi:10.1107/S1600577520011753

[6] S. Richter *et al.*, "First magnetic experience with APPLE X knot undulators for SLS 2.0", in *Proc. 16th Int. Particle Accel. Conf. (IPAC'25)*, Taipei, Taiwan, Jun. 2025, pp. 1315–1318. doi:10.18429/JACoW-IPAC2025-TUPM068

[7] S. Bettoni, M. Böge, B. Riemann, T. Schmidt, and B. Diviacco, "Impact of the insertion devices on the SLS 2.0 dynamic aperture", in *Proc. 13rd Int. Particle Accel. Conf. (IPAC'23)*, Venice, Italy, May 2023, pp. 1691–1694. doi:10.18429/JACoW-IPAC2023-TUPA166

[8] RADIA code, http://www.esrf.eu/Accelerators/Groups/InsertionDevices/Software/Radia.

[9] S. Bettoni, "Reduction of the integrated odd multipoles in periodic magnets", *Phys. Rev. Spec. Top. Accel. Beams*, vol. 10, p. 042401, Apr. 2007. doi:10.1103/PhysRevSTAB.10.042401

[10] S. Bettoni, S. Guiducci, M. Preger, and P. Raimondi, "Experimental validation for the compensation method of nonlinearities in periodic magnets", *Phys. Rev. Spec. Top. Accel. Beams*, vol. 17, p. 102401, Oct. 2014. doi:10.1103/PhysRevSTAB.17.102401.

[11] H. Grote and F. Schmidt, "MAD-X: An Upgrade from MAD8" in *Proc. Particle Accel. Conf. (PAC'03)*, Portland, OR, USA, May 2003, paper FPAG014, pp. 3497–3499.

[12] J. Laskar, C. Froeschlé, and A. Celletti, "The measure of chaos by the numerical analysis of the fundamental frequencies. Application to the standard mapping", *Physica D: Nonlinear Phenom.*, vol. 56, nos. 2–3, pp. 253-–269, 1992. doi:10.1016/0167-2789(92)90028-L

[13] K. Paraschou, S. Kostoglou, and D. Pellegrini, "Nafflib", https://github.com/PyCOMPLETE/NAFFlib.

[14] P. Zisopoulos, Y. Papaphilippou, and J. Laskar, "Refined betatron tune measurements by mixing beam position data", *Phys. Rev. Accel. Beams*, vol. 22, p. 071002, 2019, doi:10.1103/PhysRevAccelBeams.22.071002

[15] B. Keil, *et al.*, "Development of the SLS 2.0 BPM system", in *Proc. Int. Beam Instrumentation Conf. (IBIC'23)*, Saskatoon, SK, Canada, Sep. 2023, pp. 15–18, doi:10.18429/JACoW-IBIC2023-MO3C03